Effects of counter-rotating-wave terms on the noisy frequency estimation

Ze-Zhou Zhang ● and Wei Wu[*]

Key Laboratory of Theoretical Physics of Gansu Province and Lanzhou Center for Theoretical Physics,
Lanzhou University, Lanzhou 730000, China

We investigate the problem of estimating the tunneling frequency of a two-level atomic system embedded in a dissipative environment by employing a numerically rigorous hierarchical equations-of-motion method. The effect of counter-rotating-wave terms on the attainable precision of the noisy quantum metrology is systematically studied beyond the usual framework of perturbative treatments. We find the counter-rotating-wave terms are able to boost the noisy quantum metrological performance in the intermediate- and strong-coupling regimes, whether the dissipative environment is composed of bosons or fermions. The results presented in this paper may pave the way to design a high-precision quantum estimation scenario under practical decoherence.

I. INTRODUCTION

Quantum parameter estimation is a rapidly developing research field, which has many potential applications from gravitational-wave detection [1,2], quantum radar [3,4], and quantum illumination [5,6] to various ultrasensitive quantum thermometries [7–9] and magnetometers [10,11]. As demonstrated in many previous theoretical and experimental studies, using quantum coherence [12], quantum entanglement [13–15], quantum squeezing [16–18], and quantum criticality [19–22], the performance of quantum metrology can surpass the so-called shot-noise limit or standard quantum limit, which is usually achieved in classical metrological schemes.

Unfortunately, the superiority of quantum metrology is commonly destroyed by decoherence [17,23–30], which is induced by the inevitable interaction with the surrounding environment. For example, Ref. [17] reported that the Zeno-limit-type scaling relation, which is generated by the resource of quantum squeezing in the noiseless case, is degraded into the shot-noise limit under the influence of decoherence. In this sense, in any practical scheme, the decoherence should be carefully taken into account, which gives rise to the development of the so-called noisy quantum metrology [27].

However, almost all the present studies of noisy quantum metrology have restricted their attention to the bosonic environment situation with the pure dephasing mechanism [23,26,31,32] or the rotating-wave approximation (RWA) [33–35]. On the other hand, the counter-rotating-wave terms play a significant role in the atomic spontaneous emission [36], the quantum Zeno and anti-Zeno effects [37,38] and the non-Markovianity in open quantum systems [39,40]. A question is naturally raised here: what influence does the counter-rotating-wave terms have on the estimation precision of noisy quantum metrology? To address the above concern,

with the help of the nonperturbative hierarchical equations-of-motion (HEOM) method [41–47], we go beyond the usual RWA treatment and investigate the performance of estimating the frequency of a two-level system which interacts with a bosonic or fermionic environment.

This paper is organized as follows. In Sec. II, we first recall some basic concepts, mainly about the classical and quantum Fisher information, in the quantum parameter estimation theory. In Sec. III, we propose our noisy quantum metrology scheme and outline our methodology. The effect of the counter-rotating-wave terms on our metrological precision is analyzed in Sec. IV. Some related discussion and the main conclusions of this paper are given in Sec. V. In several Appendixes, we provide some additional details about the HEOM method as well as the other two additional dynamical approaches. Throughout the paper, we set $\hbar = k_{\mathrm{B}} = 1$.

II. QUANTUM PARAMETER ESTIMATION

Generally, in a typical quantum metrology scheme, the parameter of interest, say, θ in this section, is encoded into the state of a quantum system (acting as a probe) via a unitary or nonunitary dynamical process. Then, the information about θ can be extracted from the θ-dependent state ϱ_θ via repeated quantum measurements. In the above scenario, the metrological precision with respect to a given measurement scheme is constrained by the famous Cramér-Rao bound [48–50]

$$\delta^2\theta \geqslant \frac{1}{\upsilon \mathcal{F}_{\mathrm{C}}}, \tag{1}$$

where $\delta^2\theta$ denotes the variance of the derived estimator, υ is the number of repeated measurements (we set $\upsilon = 1$ for the sake of consistence in this paper), and $\mathcal{F}_{\mathrm{C}}$ is the classical Fisher information (CFI) corresponding to the selected measurement scheme. To perform such a measurement in the theory of quantum mechanics, one needs to construct a set of positive operator-valued measures $\{\hat{\Pi}_u\}$, which satisfy $\sum_u \hat{\Pi}_u^\dagger \hat{\Pi}_u = \hat{\mathbf{1}}$ with discrete measurement outcomes $\{u\}$. For

────────
[*]wuw@lzu.edu.cn

an arbitrary θ-dependent state ϱ_θ, the measurement operator $\hat{\Pi}_u$ yields an outcome u with a corresponding probability distribution $p(u|\theta) = \mathrm{Tr}(\hat{\Pi}_u \varrho_\theta \hat{\Pi}_u^\dagger)$. With all the probabilities from $\{\hat{\Pi}_u\}$ at hand, the CFI can be computed via [48–50]

$$\mathcal{F}_\mathrm{C} = \sum_u p(u|\theta) \left[\frac{\partial}{\partial \theta} \ln p(u|\theta) \right]^2. \qquad (2)$$

From Eq. (2), one can find the value of CFI strongly relies on the choice of measurement operators. Running over all the possible measurement schemes, one can prove that the ultimate metrological precision is bounded by the following quantum Cramér-Rao inequality [51]:

$$\delta^2\theta \geqslant \frac{1}{\upsilon \mathcal{F}_\mathrm{Q}}, \qquad (3)$$

where $\mathcal{F}_\mathrm{Q} \equiv \mathrm{Tr}(\hat{\varsigma}^2 \varrho_\theta)$, with $\hat{\varsigma}$ determined by $\partial_\theta \varrho_\theta = \frac{1}{2}(\hat{\varsigma}\varrho_\theta + \varrho_\theta \hat{\varsigma})$, is the so-called quantum Fisher information (QFI). Specially, if ϱ_θ is a two-dimensional density matrix in the Bloch representation, namely, $\varrho_\theta = \frac{1}{2}(\mathbf{1}_2 + \vec{r} \cdot \vec{\sigma})$, with $\vec{r}$ being the Bloch vector and $\vec{\sigma} \equiv (\hat{\sigma}_x, \hat{\sigma}_y, \hat{\sigma}_z)$ being the vector of Pauli matrices, the QFI can be easily calculated via [51,52]

$$\mathcal{F}_\mathrm{Q} = |\partial_\theta \vec{r}|^2 + \frac{(\vec{r} \cdot \partial_\theta \vec{r})^2}{1 - |\vec{r}|^2}. \qquad (4)$$

If ϱ_θ is a pure state, Eq. (4) reduces to $\mathcal{F}_\mathrm{Q} = |\partial_\theta \vec{r}|^2$.

Physically speaking, the QFI describes the most statistical information in ϱ_θ, while the CFI denotes the statistical message extracted from the selected measurement scheme. Thus, one can immediately conclude that $\mathcal{F}_\mathrm{Q} \geqslant \mathcal{F}_\mathrm{C}$. When the selected measurement scheme is the optimal one, $\mathcal{F}_\mathrm{C}$ can be saturated to $\mathcal{F}_\mathrm{Q}$. Unfortunately, there is no general way to find the optimal measurement operator, which has an explicit physical meaning. In this sense, designing the physically optimal measurement scheme, which can saturate the best attainable precision bounded by the QFI, is important in the study of quantum metrology.

III. NOISY QUANTUM FREQUENCY ESTIMATION

As discussed in several previous articles [23,26,32,33,53], in the ideal noiseless case, the information of the estimated frequency, denoted by Δ in this paper, can be encoded to the state of a two-level atomic system, which acts as a quantum probe, via a unitary dynamics: $\varrho_\Delta = \varrho(t) = e^{-it\hat{H}_\mathrm{s}} \varrho(0) e^{it\hat{H}_\mathrm{s}}$, with $\hat{H}_\mathrm{s} = \frac{1}{2}\Delta\hat{\sigma}_x$ being the Hamiltonian of the probe. However, such a unitary encoding scheme breaks down if the environmental influence is taken into account. In the noisy case, the encoding process is realized by a nonunitary dynamics $\varrho_\Delta = \varrho_\mathrm{s}(t) = \mathrm{Tr}_\mathrm{e}[e^{-it\hat{H}} \varrho_\mathrm{se}(0) e^{it\hat{H}}]$, where $\varrho_\mathrm{s}(t)$ denotes the reduced density operator of the probe by tracing out the environmental degrees of freedom and $\hat{H}$ is the total Hamiltonian of the probe plus the environment. In this paper, we assume $\hat{H}$ has the following general form [40,54–56]:

$$\hat{H} = \hat{H}_\mathrm{s} + \sum_k \omega_k \hat{c}_k^\dagger \hat{c}_k + \sum_k (g_k^* \hat{\sigma}_- \hat{c}_k^\dagger + g_k \hat{\sigma}_+ \hat{c}_k)$$

$$+ \chi \sum_k (g_k^* \hat{\sigma}_+ \hat{c}_k^\dagger + g_k \hat{\sigma}_- \hat{c}_k), \qquad (5)$$

where $\hat{c}_k$ and $\hat{c}_k^\dagger$ are the annihilation and creation operators of the kth environmental mode with frequency ω_k, respectively. If $\hat{c}_k$ and $\hat{c}_k^\dagger$ satisfy the canonical commutation relations $[\hat{c}_k, \hat{c}_{k'}^\dagger] = \delta_{kk'}$, one can deem that the environment is composed of bosons. On the other hand, if $\hat{c}_k$ and $\hat{c}_k^\dagger$ obey $\{\hat{c}_k, \hat{c}_{k'}^\dagger\} = \delta_{kk'}$, then the environment is a fermionic environment. Operators $\hat{\sigma}_\pm$ are defined as $\hat{\sigma}_- = \hat{\sigma}_+^\dagger \equiv |-\rangle\langle+|$, with $|\pm\rangle$ being the eigenstates of the Pauli-x operator, i.e., $\hat{\sigma}_x|\pm\rangle = \pm|\pm\rangle$, and g_k are complex numbers quantifying the coupling strength between the quantum probe and the kth environmental mode. The dimensionless parameter χ is a real number, satisfying $\chi \in [0, 1]$, and characterizes the weight of counter-rotating-wave terms in the interaction Hamiltonian. When $\chi = 0$, all the counter-rotating-wave terms are removed, and $\hat{H}$ reduces to the damped Jaynes-Cummings model [33–35,53]. When $\chi = 1$, all the contributions of the counter-rotating-wave terms are taken into consideration, and the Hamiltonian is totally beyond the RWA. By introducing such a parameter, a bridge between the RWA regime and the non-RWA regime can be built, which helps us to get a deeper understanding of the effect of counter-rotating-wave terms on the parameter estimation in a dissipative environment.

To obtain the information of the estimated frequency, one needs to monitor the reduced density operator of the probe, namely, $\varrho_\mathrm{s}(t)$. In this paper, we adopt the HEOM method [41–47], which can provide a numerically rigorous result, to solve this problem (see Appendix A for more details). As benchmarks, we also employ two other approaches, the Zwanzig-Nakajima master-equation technique (see Refs. [57,58] and Appendix B) and the RWA treatment (see Appendix C), to investigate the reduced dynamics of the probe. Together with the purely numerical results from the HEOM, these two additional methods can make our conclusion more persuasive.

In this paper, we assume the initial state of the whole system is given by

$$\varrho_\mathrm{se}(0) = \varrho_\mathrm{s}(0) \otimes \varrho_\mathrm{e} = |\psi_\mathrm{s}(0)\rangle\langle\psi_\mathrm{s}(0)| \bigotimes_k |0_k\rangle\langle0_k|, \qquad (6)$$

where $|\psi_\mathrm{s}(0)\rangle = \cos\phi|+\rangle + \sin\phi|-\rangle$ and $|0_k\rangle$ denotes the vacuum state of the kth environmental mode. The spectral density of the environment $J(\omega)$, which is defined by $J(\omega) = \sum_k |g_k|^2 \delta(\omega - \omega_k)$, has a Lorentzian form,

$$J(\omega) = \frac{1}{2\pi} \frac{\gamma\lambda^2}{(\omega - \Delta)^2 + \lambda^2}, \qquad (7)$$

where λ defines the spectral width and γ can be approximately interpreted as the probe-environment coupling strength. The Lorentzian spectral density has a clear Markovian–non-Markovian boundary [30,59–61] and can give rise to an Ornstein-Uhlenbeck-type environmental correlation function, which guarantees the feasibility of the HEOM algorithm (see Appendix A for details).

As long as $\varrho_\mathrm{s}(t)$ is obtained, the CFI and the QFI can be calculated by making use of Eqs. (2) and (4), respectively. During the purely numerical calculations, one needs to handle the first-order derivative of the parameter Δ, say, $\partial_\Delta \vec{r}$ in Eq. (4). In this paper, the first-order derivative for an arbitrary Δ-dependent function f_Δ is numerically done by adopting the
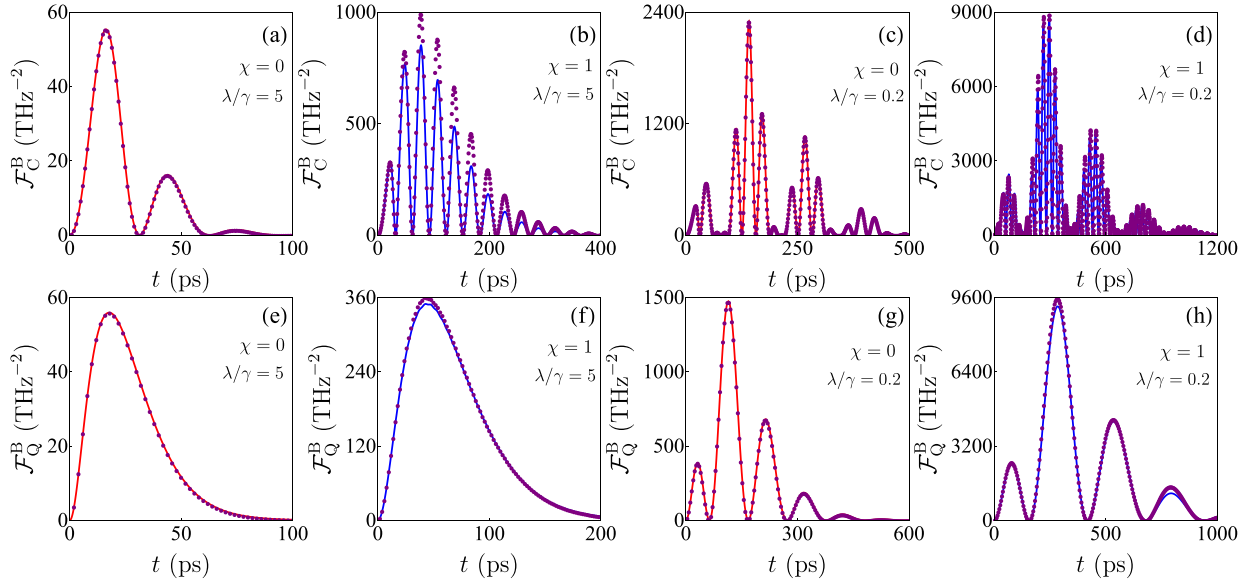
FIG. 1. The dynamics of the CFI (top panels) and the QFI (bottom panels) in the Markovian regime ($\lambda/\gamma = 5$) and the non-Markovain regime ($\lambda/\gamma = 0.2$). The red solid lines are analytical results from the RWA treatment, namely, $\chi = 0$. The blue solid lines are obtained with the Zwanzig-Nakajima master-equation approach. The HEOM results are represented by purple circles. The coupling strengths are chosen as (a) $\gamma = 0.1$ cm^{-1}, (b) $\gamma = 0.02$ cm^{-1}, (c) $\gamma = 0.08$ cm^{-1}, and (d) $\gamma = 0.04$ cm^{-1} with $\Delta = 0.1$ THz and $\phi = \pi/4$ and (e) $\gamma = 0.1$ cm^{-1}, (f) $\gamma = 0.04$ cm^{-1}, (g) $\gamma = 0.1$ cm^{-1}, and (h) $\gamma = 0.04$ cm^{-1} with $\Delta = 10$ THz and $\phi = \pi/4$.

following finite-difference method:

$$\partial_\Delta f_\Delta \simeq \frac{-f_{\Delta+2\delta} + 8f_{\Delta+\delta} - 8f_{\Delta-\delta} + f_{\Delta-2\delta}}{12\delta}. \tag{8}$$

We set $\delta/\Delta = 10^{-6}$, which provides very good accuracy.

IV. RESULTS

In this section, we try to address the effect of counter-rotating-wave terms on the noisy quantum frequency estimation. To obtain the CFI, the measurement operators in this paper are chosen as $\hat{\Pi} = \{|e\rangle\langle e|, |g\rangle\langle g|\}$, with $|e, g\rangle$ being the eigenstates of the Pauli-z operator. In the ideal noiseless case, the CFI with respect to the selected measurement scheme is $\mathcal{F}_C^{\text{ideal}} = t^2$, which is completely saturated to the QFI (see Appendix C). This result means the choice of the measurement scheme is the optimal one. Moreover, our measurement scheme is mathematically equivalent to performing standard Ramsey spectroscopy [13,23,53], which is commonly employed to estimate the phases (or external magnetic field) of cold atomic systems. As the detailed expositions of a typical Ramsey interferometer setup for a two-level system [13,23,53], the uncertainty of estimating the parameter Δ from the error-propagation formula is in full accord with that of the CFI obtained from Eq. (2). Thus, it is quite natural to generalize the above measurement scheme to the noisy case and evaluate the environmental influences on its performance. We find that, in the noisy situation, although the selected measurement scheme cannot completely saturate the ultimate bound given by the quantum Cramér-Rao theorem [see the numerical results in Figs. 2(a)–2(c) and 3(a)–3(c)], the corresponding CFI is in qualitative agreement with the QFI in the non-Markovian and strong-coupling regimes.

A. The bosonic environment case

In Fig. 1, we plot the dynamics of the CFI and the QFI for $\chi = 0$ and $\chi = 1$, including both the Markovian ($\lambda/\gamma \to \infty$) and non-Markovian ($\lambda/\gamma \to 0$) cases. From Fig. 1, we can see both the CFI and the QFI gradually increase from zero to their maximum values with certain oscillations. Such oscillations are quite dramatic in non-Markovian regimes and may be linked to the backflow of information from the environment back to the probe [30,33,61]. As the encoding time becomes longer, both the CFI and the QFI begin to decrease and eventually vanish in the long-encoding-time limit. These results can be physically understood as the competition between the encoding process and the decoherence in noisy quantum metrology [29,30,35]. At the beginning, the nonunitary encoding process generates the information of Δ in $\varrho_s(t)$, which leads to the increase of the CFI (QFI) from zero. However, as the encoding time becomes longer, the message about Δ inevitably leaks to the environment and is eventually destroyed by the decoherence. Our result suggests there exists an optimal encoding time which can maximize the value of CFI (QFI). In Figs. 2(a)–2(c), we plot the maximal CFI (QFI) with respect to the encoding time as a function of χ. We can see the optimal CFI (QFI) monotonously increases as the value of χ becomes large, which means the counter-rotating-wave terms can effectively boost the performance of our noisy quantum metrology in the strong-coupling regime. On the other hand, we define the quantities

$$\delta\mathcal{F}_\ell^B \equiv \max_t \mathcal{F}_\ell^B - \max_t \mathcal{F}_\ell^{\text{RWA}} \tag{9}$$

to quantify the effect of the counter-rotating-wave terms on the metrological precision. Here, the superscript $\ell = C$ or Q implies the CFI or the QFI, and $\mathcal{F}_\ell^B$ and $\mathcal{F}_\ell^{\text{RWA}}$ denote the Fisher information for $\chi = 1$ and $\chi = 0$, respectively. As long
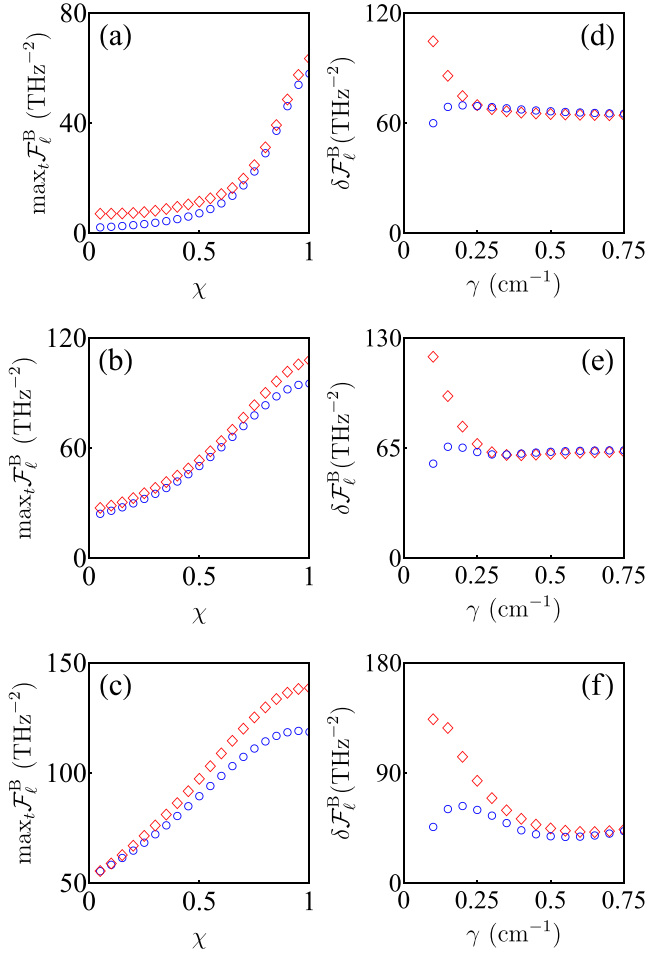
FIG. 2. Left: the optimal Fisher information with respect to the encoding time is plotted as a function of χ for the bosonic environment case. Right: the modification of the Fisher information induced by the counter-rotating-wave terms is displayed as a function of γ for the bosonic environment case. Parameters are chosen as (a) $\lambda/\gamma = 0.8$, (b) $\lambda/\gamma = 2$, and (c) $\lambda/\gamma = 3$ with $\lambda = 0.32$ cm^{-1} and (d) $\lambda/\gamma = 1.5$, (e) $\lambda/\gamma = 1$, and (f) $\lambda/\gamma = 0.5$ with $\chi = 1$. The red diamonds and blue circles are, respectively, the QFI ($\ell = $ Q) and the CFI ($\ell = $ C) predicted by the HEOM method. Here, we mainly focus on the non-Markovian and strong-coupling regimes in which the effect of counter-rotating-wave terms is significant. The other parameters are $\Delta = 0.1$ THz and $\phi = \pi/4$.

as $\delta\mathcal{F}_\ell^B > 0$, one can conclude that the counter-rotating-wave terms play a positive role in improving the metrological precision. In Figs. 2(d)–2(f), we plot $\delta\mathcal{F}_\ell^B$ as a function of the
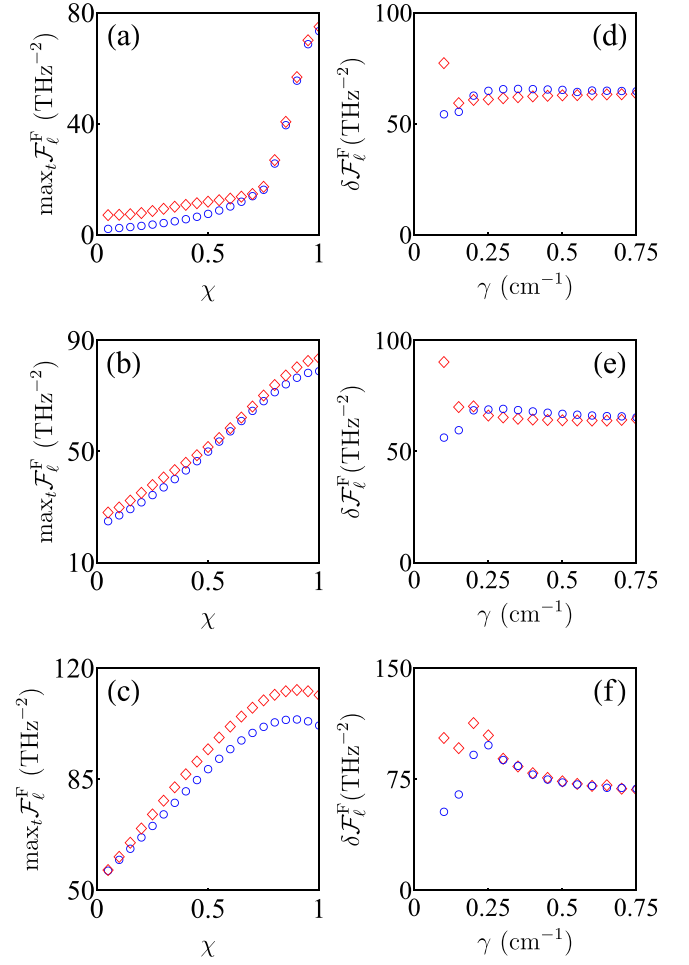
FIG. 3. The same as Fig. 2, but in the fermionic environment case.

coupling constant γ. As we can see from Figs. 2(d)–2(f), $\delta\mathcal{F}_\ell^B$ remains positive in the entire range of intermediate- and strong-coupling regimes (say, $0.10 \leqslant \gamma \leqslant 0.75$ cm^{-1} in Fig. 2). In Table I and Fig. 4(c), we show the Fisher information with and without the RWA in the weak-coupling regime, which demonstrates $\max_t \mathcal{F}_Q^B > \max_t \mathcal{F}_Q^{RWA}$ as well. These results mean the consideration of counter-rotating-wave terms can provide a larger QFI. However, we also notice that $\max_t \mathcal{F}_C^B$ can be smaller than $\max_t \mathcal{F}_C^{RWA}$ when γ is very small. Such a deviation from that of the QFI situation is probably induced by the fact that the selected measurement scheme $\hat{\Pi} = \{|e\rangle\langle e|, |g\rangle\langle g|\}$ is not the optimal one in the noisy

TABLE I. The Fisher information (QFI and CFI) versus the coupling strength in the weak-coupling regime. Here, $\mathbb{R}_B$ is defined as $\mathbb{R}_\ell^B \equiv \max_t \mathcal{F}_\ell^{RWA} / \max_t \mathcal{F}_\ell^B$. Other parameters are the same as in Fig. 2.

| γ (cm^{-1})	0.00	0.01	0.02	0.03	0.04	0.05	0.06	0.07	0.08	0.09
$\mathbb{R}_Q^B$ ($\lambda/\gamma = 1.5$)	1.0000	0.9733	0.9294	0.9147	0.9524	0.8591	0.7122	0.6115	0.5381	0.4818
$\mathbb{R}_Q^B$ ($\lambda/\gamma = 1.0$)	1.0000	0.9536	0.9286	0.9171	0.9009	0.9467	0.7775	0.6622	0.5792	0.5169
$\mathbb{R}_Q^B$ ($\lambda/\gamma = 0.5$)	1.0000	0.9653	0.9286	0.9224	0.8786	0.8846	0.9050	0.8349	0.7205	0.6344
$\mathbb{R}_C^B$ ($\lambda/\gamma = 1.5$)	1.0000	1.0164	1.0669	1.1262	1.2134	1.0619	0.8243	0.7631	0.6994	0.6355
$\mathbb{R}_C^B$ ($\lambda/\gamma = 1.0$)	1.0000	1.0103	1.0390	1.0719	1.1493	1.2190	0.8633	0.8135	0.7597	0.7038
$\mathbb{R}_C^B$ ($\lambda/\gamma = 0.5$)	1.0000	1.0045	1.0176	1.0410	1.0535	1.1140	1.1744	1.0459	0.8518	0.8137
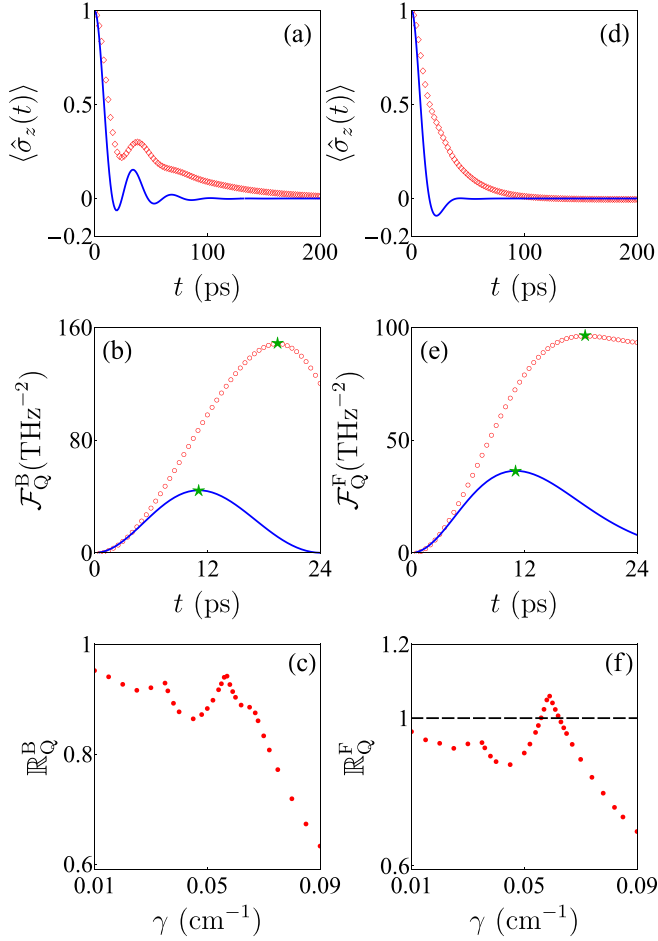
FIG. 4. The dynamics of the population difference $\langle \hat{\sigma}_z(t) \rangle$ with (blue solid lines) and without (red diamonds) RWA in the strong-coupling regime for (a) the bosonic environment case ($\gamma = 0.2$ cm^{-1} and $\lambda/\gamma = 0.5$) and (d) the fermionic environment case ($\gamma = 0.15$ cm^{-1} and $\lambda/\gamma = 1.5$). The dynamics of the QFI $\mathcal{F}_Q(t)$ with (blue solid lines) and without (red circles) RWA in the strong-coupling regime for (b) the bosonic environment case ($\gamma = 0.2$ cm^{-1} and $\lambda/\gamma = 0.5$) and (e) the fermionic environment case ($\gamma = 0.15$ cm^{-1} and $\lambda/\gamma = 1.5$). Here, the green five-point stars mark the positions of the optimal QFIs with respect to the encoding time. The ratio of $\mathbb{R}_\ell$ versus γ in the weak-coupling regime with $\lambda/\gamma = 0.5$ for (c) the bosonic environment case and (f) the fermionic environment case. The other parameters are chosen as $\Delta = 0.1$ THz and $\phi = \pi/4$.

environment. This implies the CFI cannot be completely aligned with the behavior of QFI.

B. The fermionic environment case

Almost all the existing studies of noisy quantum metrology have restricted their attention to the bosonic environment case. In this section, we generalize our study to the fermionic environment case with the help of the HEOM method (see Appendix A). We find the Fisher information in the fermionic environment has a dynamical behavior similar to that of the bosonic environment case (not shown here). Thus, by optimizing the encoding time, the maximal CFI and QFI versus χ can be obtained. As displayed in Figs. 3(a)–3(c), we can see

the metrological precision can be improved by increasing the weight of the counter-rotating-wave terms. Like in the bosonic environment case, we here define

$$\delta \mathcal{F}_\ell^{\mathrm{F}} \equiv \max_t \mathcal{F}_\ell^{\mathrm{F}} - \max_t \mathcal{F}_\ell^{\mathrm{RWA}} \tag{10}$$

as the quantity to detect the influence of the counter-rotating-wave terms on our metrological precision in the fermionic environment case, denoted with a superscript F. As displayed in Figs. 3(d)–3(f) and Table II, we confirm that $\delta \mathcal{F}_\ell^{\mathrm{F}}$ is positive in the strong-coupling regime for the fermionic environment case. These results demonstrate that the counter-rotating-wave terms are able to boost the QFI by enhancing the probe-environment coupling, whether the environment is composed of bosons or fermions. However, if γ is very small, an anomalous phenomenon of $\mathbb{R}_\ell^{\mathrm{F}} > 1$ may occur [see Table II and Fig. 4(f)].

Here, we would like to provide a possible physical explanation of why the counter-rotating-wave terms fail to improve the metrological performance in the small-γ regime. Essentially, we concentrate on the problem of noisy quantum parameter estimation, which means the decoherence induced by the system-environment coupling plays a negative role in the metrological performance. It is commonly thought that a more severe decoherence always induces a lower sensitivity because stronger noise leads to more serious damage to the ideal precision obtained in the noiseless case. On the other hand, the system-environment interactions with and without the RWA can be viewed as two completely different decoherence channels. Such a difference gives rise to distinct decay rates as well as disparate estimation accuracies. As displayed in Figs. 4(a) and 4(d), we find, in the strong-coupling regime, the inclusion of counter-rotating-wave terms can effectively inhibit decoherence. This decoherence-suppression effect was also reported in Ref. [62] and can lead to a larger $\max_t \mathcal{F}_\ell$ [see Figs. 4(b) and 4(e)]. However, as the coupling strength decreases, the influence of counter-rotating-wave terms vanishes, resulting in the above mechanism of decoherence suppression breaking down. Thus, in the weak-coupling regime, the phenomenon of quantum metrology boosted by counter-rotating-wave terms may disappear. Such an anomalous phenomenon is displayed in Fig. 4(f), from which we can see the ratio of $\mathbb{R}_Q^{\mathrm{F}}$ can be larger than 1 if γ is small.

V. DISCUSSION AND CONCLUSION

Before concluding our work, some important remarks shall be addressed here.

(i) In our work, the strength of the counter-rotating-wave terms in the interaction Hamiltonian, namely, the parameter χ, is continuously tunable for the entire range of $\chi \in [0, 1]$, which can build a bridge connecting two particular limits: totally with and without the RWA. In fact, such controllable strength of the counter-rotating-wave terms in the quantum Rabi model is called anisotropy [63–65], which leads to a much richer ground-state phase diagram [64,65] and can be used to explain the anomalous Bloch-Siegert shift in the ultrastrong-coupling regime [66]. These previous studies of the anisotropic quantum Rabi model motivate us to explore the influence of the counter-rotating-wave terms on the

TABLE II. The same as Table I, but in the fermionic environment case. Here, $\mathbb{R}_F$ is defined as $\mathbb{R}_\ell^F \equiv \max_t \mathcal{F}_\ell^{RWA} / \max_t \mathcal{F}_\ell^F$.

γ (cm^{-1})	0.00	0.01	0.02	0.03	0.04	0.05	0.06	0.07	0.08	0.09
$\mathbb{R}_Q^F$ ($\lambda/\gamma = 0.5$)	1.0000	0.9657	0.9341	0.9326	0.8846	0.9079	1.0435	0.8907	0.7991	0.6955
$\mathbb{R}_Q^F$ ($\lambda/\gamma = 1.0$)	1.0000	0.9577	0.9411	0.9383	0.9760	1.0099	0.8440	0.7301	0.6476	0.5854
$\mathbb{R}_Q^F$ ($\lambda/\gamma = 1.5$)	1.0000	0.9733	0.9655	0.9720	1.1567	0.9321	0.7861	0.6842	0.6119	0.5558
$\mathbb{R}_C^F$ ($\lambda/\gamma = 0.5$)	1.0000	1.0019	1.0058	1.0151	1.0036	1.0286	1.0846	1.0761	0.8291	0.7891
$\mathbb{R}_C^F$ ($\lambda/\gamma = 1.0$)	1.0000	1.0094	1.0298	1.0438	1.1307	1.2738	0.8496	0.8008	0.7496	0.6975
$\mathbb{R}_C^F$ ($\lambda/\gamma = 1.5$)	1.0000	1.0234	1.0785	1.1280	1.3398	1.0534	0.8209	0.7654	0.7085	0.6520

metrological precision by introducing the engineered tunable parameter χ.

(ii) Compared with the widely accepted interaction Hamiltonian between a two-level spin and a bosonic environment, the form of the spin-fermion interaction still remains controversial. The spin-fermion model considered in this paper is the most straightforward generalization of the well-accepted spin-boson model and can be regarded as a toy model. However, it is necessary to emphasize that such a spin-fermion model is not merely of academic interest. It may be used to describe certain physical phenomena, say, the magnetism of the weak-moment heavy-fermion compound UR$_2$Si$_2$ [67,68].

(ii) Although the theoretical model and the numerical tool are the same as those in Ref. [40], the central goal of our work is utterly different from that of Ref. [40]. Our paper concentrates on a concrete physical problem, while Ref. [40] is much closer to a methodology article discussing the HEOM method. More importantly, we here investigate an alternative topic, which means the physical conclusion in Ref. [40] cannot be straightforwardly applied to our present paper.

(iv) Simulating the exact non-Markovian dissipative dynamics of an open quantum system in the strong-coupling regime is difficult. As reported in Refs. [69–74], the so-called negative-frequency phenomenon may appear in the strong-coupling regime, which leads to isolated eigenenergies in the energy spectrum (the bound-state effect) [70–72]. The appearance of negative frequencies can lead to a long-lived coherence [69,70,72] as well as the breakdown of canonical thermalization [71,74], which cannot be predicted by the common quantum master-equation approach. However, to the best of our knowledge, such a negative-frequency phenomenon usually occurs in the unbiased spin-boson model with the RWA [70,72] or the quantum Brownian motion (the Caldeira-Leggett model) without adding the counter term [73,74]. For the model considered in this paper (a Lorentzian spin-boson model totally beyond the RWA), the negative-frequency phenomenon has not been reported. Excluding the negative-frequency problem, we believe the numerical correctness from the HEOM method can be fully guaranteed.

In summary, using the numerically rigorous HEOM method, we investigated the exact reduced dynamics of a two-level system coupled to a dissipative bosonic or fermionic environment. With these results, we analyzed the influence of counter-rotating-wave terms on the performance of noisy parameter estimation beyond the usual weak-coupling treatment. It was revealed that the counter-rotating-wave terms can effectively enhance the metrological precision in the non-Markovian and strong-coupling regimes, regardless of whether the dissipative environment is composed of bosons or fermions. Our results may have certain applications in quantum metrology and quantum sensing.

APPENDIX A: THE HEOM METHOD

In this Appendix, we briefly sketch the HEOM method following the detailed expositions in Refs. [40,46,47,75]. Let us consider a general quantum dissipative system whose Hamiltonian can be described by

$$\hat{H} = \hat{H}_s + \sum_k \omega_k \hat{c}_k^\dagger \hat{c}_k + \sum_k (g_k^* \hat{L} \hat{c}_k^\dagger + g_k \hat{L}^\dagger \hat{c}_k), \quad \text{(A1)}$$

where $\hat{L}$ is the quantum probe's operator coupled to its surrounding dissipative environment. Taking $\hat{L} = \hat{\sigma}_- + \chi \hat{\sigma}_+$, Eq. (5) in the main text can be recovered. The dynamics of the Hamiltonian $\hat{H}$ is governed by the common Schrödinger equation. By introducing the bosonic or the fermionic coherent state $|\mathbf{z}\rangle \equiv \bigotimes_k |z_k\rangle$, with $\hat{c}_k|z_k\rangle = z_k|z_k\rangle$, one can recast the standard Schrödinger equation into the following non-Markovian quantum state diffusion [76–78]:

$$\frac{\partial}{\partial t}|\psi_t(\mathbf{z}^*)\rangle = -i\hat{H}_s|\psi_t(\mathbf{z}^*)\rangle + \hat{L}\mathbf{z}_t^*|\psi_t(\mathbf{z}^*)\rangle$$
$$- \hat{L}^\dagger \int_0^t d\tau C(t-\tau)\frac{\delta}{\delta \mathbf{z}_\tau^*}|\psi_t(\mathbf{z}^*)\rangle, \quad \text{(A2)}$$

where $|\psi_t(\mathbf{z}^*)\rangle$ is the wave function in the coherent-state representation. The stochastic variable (random noise) $\mathbf{z}_t \equiv i\sum_k g_k e^{-i\omega_k t} z_k$ satisfies $\mathcal{M}\{\mathbf{z}_t\} = \mathcal{M}\{\mathbf{z}_t^*\} = 0$ and $\mathcal{M}\{\mathbf{z}_t \mathbf{z}_\tau^*\} = C(t-\tau) \equiv \sum_k |g_k|^2 e^{-i\omega_k(t-\tau)}$, where $\mathcal{M}\{\cdots\}$ denotes the statistical mean over all the possible stochastic processes and $C(t)$ is the environmental correction function. By far, no approximation is invoked, which means the non-Markovian quantum state diffusion equation given by Eq. (A2) is exact. However, Eq. (A2) is difficult to solve due to the time-nonlocal functional derivative term [46,47].

Fortunately, for the Lorentzian spectral density considered in this paper, $C(t)$ is an Ornstein-Uhlenbeck-type correlation function; namely, $C(t)$ can be expressed as an exponential function: $C(t) = \alpha e^{-\beta t}$, with $\alpha = \frac{1}{2}\gamma\lambda$ and $\beta = \lambda + i\Delta$. Using this particularity, the HEOM algorithm can be realized [40,46,47,75]. By introducing auxiliary operators

$\varrho_t^{(m,n)} \equiv \mathcal{M}\{|\psi_t^{(m)}(\mathbf{z}^*)\rangle \langle \psi_t^{(n)}(\mathbf{z}^*)|\}$, with

$$|\psi_t^{(m)}(\mathbf{z}^*)\rangle \equiv \left[\int_0^t d\tau C(t-\tau)\frac{\delta}{\delta \mathbf{z}_\tau^*}\right]^m |\psi_t(\mathbf{z}^*)\rangle, \qquad (A3)$$

the non-Markovian quantum state diffusion equation can be reexpressed as the following HEOM [40,46,47,75]:

$$\frac{d}{dt}\varrho_t^{(m,n)} = (-i\hat{H}_s^\times - m\beta - n\beta^*)\varrho_t^{(m,n)}$$
$$+ m\alpha\hat{L}\varrho_t^{(m-1,n)} + n\alpha^*\varrho_t^{(m,n-1)}\hat{L}^\dagger$$
$$- \hat{L}^{\dagger\times}\varrho_t^{(m+1,n)} + \hat{L}^\times\varrho_t^{(m,n+1)}, \qquad (A4)$$

where $\hat{X}^\times\hat{Y} \equiv \hat{X}\hat{Y} - \hat{Y}\hat{X}$ and $\varrho_t^{(0,0)}$ is the reduced density operator of the probe. Similarly, the HEOM of the spin-fermion model is given by [40,75]

$$\frac{d}{dt}\varrho_t^{(m,n)} = (-i\hat{H}_s^\times - m\beta - n\beta^*)\varrho_t^{(m,n)}$$
$$+ \Theta(m)\alpha\hat{L}\varrho_t^{(m-1,n)} + \Theta(n)\alpha^*\varrho_t^{(m,n-1)}\hat{L}^\dagger$$
$$+ \left[(-1)^n\varrho_t^{(m+1,n)}\hat{L}^\dagger - \hat{L}^\dagger\varrho_t^{(m+1,n)}\right]$$
$$+ \left[(-1)^m\hat{L}\varrho_t^{(m,n+1)} - \varrho_t^{(m,n+1)}\hat{L}\right], \qquad (A5)$$

where $\Theta(x) \equiv x \bmod 2$ and the auxiliary operators are defined as $\varrho_t^{(m,n)} = \mathcal{M}\{|\psi_t^{(m)}(\mathbf{z}^*)\rangle \langle \psi_t^{(n)}(-\mathbf{z}^*)|\}$.

The initial-state conditions of the auxiliary operators are $\varrho_t^{(0,0)} = \varrho_s(0)$ and $\varrho_t^{(m>0,n>0)} = 0$. In numerical simulations, we need to truncate the hierarchical equations. In practice, we choose a sufficiently large integer N and set $\varrho_t^{(m,n)}$ with $m + n > N$ to zero. Then, $\varrho_t^{(m,n)}$ with $m + n \leqslant N$ form a closed set of ordinary differential equations which can be numerically solved by using the well-developed Runge-Kutta algorithm.

APPENDIX B: ZWANZIG-NAKAJIMA MASTER EQUATION

In the special case $\chi = 1$, $\hat{H}$ reduces to the standard spin-boson model, whose reduced dynamics can be captured by the famous Zwanzig-Nakajima master equation [79,80]

$$\frac{\partial}{\partial t}\varrho_s(t) = -i\hat{\mathcal{L}}_s\varrho_s(t) - \int_0^t d\tau \hat{\Sigma}(t-\tau)\varrho_s(\tau), \qquad (B1)$$

where we have used the Born approximation $\hat{\mathcal{L}}_x\hat{\mathcal{O}} = \hat{H}_x^\times\hat{\mathcal{O}}$, where x = s, e, i are the Liouvillian operators corresponding to the probe, the environment, and the probe-environment interaction Hamiltonian, respectively. Here, $\hat{\Sigma}(t)$ is the self-energy superoperator. If the probe-environment coupling is weak, $\hat{\Sigma}(t)$ can be approximately written as [57,58]

$$\hat{\Sigma}(t) \simeq \mathrm{Tr}_e[\hat{\mathcal{L}}_i e^{-it(\hat{\mathcal{L}}_s + \hat{\mathcal{L}}_e)}\hat{\mathcal{L}}_i\varrho_e]. \qquad (B2)$$

In the Bloch representation, the Zwanzig-Nakajima master equation can be expressed as $\partial_t\vec{r}(t) = \mathfrak{S}(t) \diamond \vec{r}(t)$, where $\diamond$ denotes the convolution and

$$\mathfrak{S}(t) = \begin{bmatrix} -\mathcal{A}(t) & 0 & 0 \\ 0 & -\mathcal{B}(t) & -\Delta\delta(t) \\ 0 & \Delta\delta(t) & 0 \end{bmatrix}, \qquad (B3)$$

with $\mathcal{A}(t) = 4\cos(\Delta t)C(t)$ and $\mathcal{B}(t) = 4C(t)$. By means of the Laplace transform, one can find

$$\tilde{r}_i(\zeta) \equiv \int_0^\infty dt\, r_i(t)e^{-\zeta t} = \sum_j \mathfrak{F}_{ij}(\zeta)r_j(0), \qquad (B4)$$

where $i, j = x, y, z$. The nonvanishing terms of $\mathfrak{F}_{ij}(\lambda)$ are given by

$$\mathfrak{F}_{xx}(\zeta) = [\zeta + \tilde{\mathcal{A}}(\zeta)]^{-1}, \qquad (B5)$$

$$\mathfrak{F}_{yy}(\zeta) = \left[\zeta + \tilde{\mathcal{B}}(\zeta) + \frac{\Delta^2}{\zeta}\right]^{-1}, \qquad (B6)$$

$$\mathfrak{F}_{zz}(\zeta) = [1 + \zeta^{-1}\tilde{\mathcal{B}}(\zeta)]\mathfrak{F}_{yy}(\zeta), \qquad (B7)$$

$$\mathfrak{F}_{yz}(\zeta) = -\mathfrak{F}_{zy}(\zeta) = -\Delta\zeta^{-1}\mathfrak{F}_{yy}(\zeta). \qquad (B8)$$

Then, for an arbitrary given initial state, the reduced dynamics of the Bloch vector $\vec{r}(t)$ can be completely determined by Eq. (B4) with the help of the inverse Laplace transform.

APPENDIX C: THE RWA CASE

In the special case with $\chi = 0$, the RWA completely removes the counter-rotating-wave terms in $\hat{H}$, resulting in the total excitation number operator $\hat{\mathcal{N}} = \hat{\sigma}_+\hat{\sigma}_- + \sum_k \hat{c}_k^\dagger\hat{c}_k$ being a constant of motion. This character leads to the spin-boson model and the spin-fermion model sharing the same reduced dynamical behavior in the RWA case [40]. As displayed in Refs. [40,59], in the basis of $\{|+\rangle, |-\rangle\}$, the exactly analytical expression of $\varrho_s(t)$ can be expressed as

$$\varrho_s(t) = \begin{bmatrix} \varrho_{++}(0)\mathcal{G}_t^2 & \varrho_{+-}(0)\mathcal{G}_t e^{-i\Delta t} \\ \varrho_{-+}(0)\mathcal{G}_t e^{i\Delta t} & 1 - \varrho_{++}(0)\mathcal{G}_t^2 \end{bmatrix}, \qquad (C1)$$

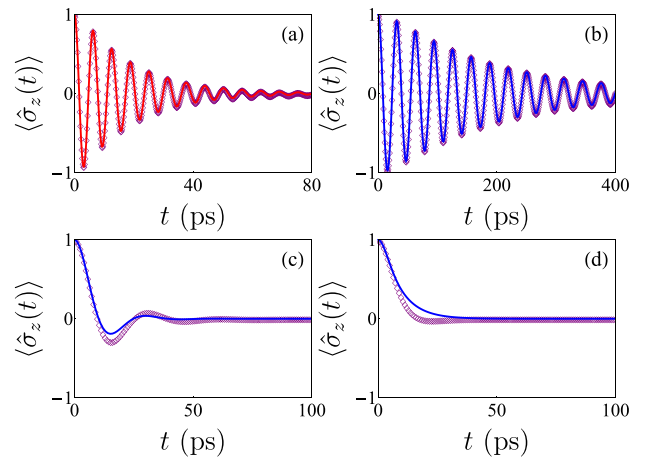FIG. 5. The dynamics of the population difference with (a) $\chi = 0$, $\gamma = 0.1$ cm^{-1}, and $\Delta = 1$ THz, (b) $\chi = 1$, $\gamma = 0.01$ cm^{-1}, and $\Delta = 0.2$ THz, (c) $\chi = 1$, $\gamma = 0.1$ cm^{-1}, and $\Delta = 0.2$ THz, and (d) $\chi = 1$, $\gamma = 0.2$ cm^{-1}, and $\Delta = 0.2$ THz. The red solid line represents the exactly analytical RWA treatment, the blue solid lines are obtained from the Zwanzig-Nakajima master-equation approach, and the purple diamonds are purely numerical results predicted by the HEOM method. The other parameters are $\lambda = 5\gamma$ and $\phi = \pi/4$.

where

$$\mathcal{G}_t = \exp\left(-\frac{1}{2}\lambda t\right)\left[\cosh\left(\frac{1}{2}\Omega t\right) + \frac{\lambda}{\Omega}\sinh\left(\frac{1}{2}\Omega t\right)\right] \tag{C2}$$

is the decoherence factor and $\Omega \equiv \sqrt{\gamma^2 - 2\gamma\lambda}$.

With Eq. (C1) at hand, the analytical expressions of CFI and QFI can be easily computed. Assuming the initial-state parameter ϕ is chosen as $\phi = \pi/4$, we find

$$\mathcal{F}_C^{\mathrm{RWA}} = \frac{t^2 \mathcal{G}_t^2 \sin^2(\Delta t)}{1 - \mathcal{G}_t^2 \cos^2(\Delta t)} \tag{C3}$$

and $\mathcal{F}_Q^{\mathrm{RWA}} = t^2 \mathcal{G}_t^2$. One can easily check that $\mathcal{F}_Q^{\mathrm{RWA}} \geqslant \mathcal{F}_C^{\mathrm{RWA}}$ because $0 \leqslant \mathcal{G}_t \leqslant 1$. Moreover, in the ideal noiseless case, we have $\mathcal{G}_t = 1$, which leads to $\mathcal{F}_C^{\mathrm{ideal}} = \mathcal{F}_Q^{\mathrm{ideal}} = t^2$. This result

means the selected measurement scheme is the optimal one in the noise-free situation.

In Fig. 5(a), we display the dynamics of the population difference $\langle\hat{\sigma}_z(t)\rangle \equiv \mathrm{Tr}_\mathrm{s}[\hat{\sigma}_z \varrho_\mathrm{s}(t)]$ from the purely numerical HEOM method. In the special case with $\chi = 0$, one can see our numerical results are completely consistent with that of the exactly analytical RWA result $\langle\hat{\sigma}_z(t)\rangle_{\mathrm{RWA}} = \mathcal{G}_t \cos(\Delta t)$. For the case with $\chi = 1$, as long as the probe-environment coupling is not too strong, our HEOM results are in good agreement with the predictions from the Zwanzig-Nakajima master-equation approach [see Figs. 5(b)–5(d)]. However, the HEOM results are believed to be more reliable because the Zwanzig-Nakajima master-equation approach neglects the higher-order probe-environment coupling terms, which are invalid in the non-Markovian and strong-coupling regimes. These results verify the feasibility and the validity of the HEOM method.

[1] M. Tse *et al.*, Quantum-Enhanced Advanced LIGO Detectors in the Era of Gravitational-Wave Astronomy, Phys. Rev. Lett. **123**, 231107 (2019).

[2] F. Acernese *et al.* (Virgo Collaboration), Increasing the Astrophysical Reach of the Advanced Virgo Detector via the Application of Squeezed Vacuum States of Light, Phys. Rev. Lett. **123**, 231108 (2019).

[3] L. Maccone and C. Ren, Quantum Radar, Phys. Rev. Lett. **124**, 200503 (2020).

[4] Z. Huang, C. Lupo, and P. Kok, Quantum-limited estimation of range and velocity, PRX Quantum **2**, 030303 (2021).

[5] S.-H. Tan, B. I. Erkmen, V. Giovannetti, S. Guha, S. Lloyd, L. Maccone, S. Pirandola, and J. H. Shapiro, Quantum Illumination with Gaussian States, Phys. Rev. Lett. **101**, 253601 (2008).

[6] F. Xu, X.-M. Zhang, L. Xu, T. Jiang, M.-H. Yung, and L. Zhang, Experimental Quantum Target Detection Approaching the Fundamental Helstrom Limit, Phys. Rev. Lett. **127**, 040504 (2021).

[7] L. A. Correa, M. Mehboudi, G. Adesso, and A. Sanpera, Individual Quantum Probes for Optimal Thermometry, Phys. Rev. Lett. **114**, 220405 (2015).

[8] K. V. Hovhannisyan, M. R. Jørgensen, G. T. Landi, Á. M. Alhambra, J. B. Brask, and M. Perarnau-Llobet, Optimal quantum thermometry with coarse-grained measurements, PRX Quantum **2**, 020322 (2021).

[9] A. Candeloro, L. Razzoli, P. Bordone, and M. G. A. Paris, Role of topology in determining the precision of a finite thermometer, Phys. Rev. E **104**, 014136 (2021).

[10] Q. Bouton, J. Nettersheim, D. Adam, F. Schmidt, D. Mayer, T. Lausch, E. Tiemann, and A. Widera, Single-Atom Quantum Probes for Ultracold Gases Boosted by Nonequilibrium Spin Dynamics, Phys. Rev. X **10**, 011018 (2020).

[11] L. Razzoli, L. Ghirardi, I. Siloi, P. Bordone, and M. G. A. Paris, Lattice quantum magnetometry, Phys. Rev. A **99**, 062330 (2019).

[12] A. Smirne, A. Lemmer, M. B. Plenio, and S. F. Huelga, Improving the precision of frequency estimation via long-time coherences, Quantum Sci. Technol. **4**, 025004 (2019).

[13] S. F. Huelga, C. Macchiavello, T. Pellizzari, A. K. Ekert, M. B. Plenio, and J. I. Cirac, Improvement of Frequency

Standards with Quantum Entanglement, Phys. Rev. Lett. **79**, 3865 (1997).

[14] T. Nagata, R. Okamoto, J. L. O'Brien, K. Sasaki, and S. Takeuchi, Beating the standard quantum limit with four-entangled photons, Science **316**, 726 (2007).

[15] L. Pezzè, A. Smerzi, M. K. Oberthaler, R. Schmied, and P. Treutlein, Quantum metrology with nonclassical states of atomic ensembles, Rev. Mod. Phys. **90**, 035005 (2018).

[16] C. M. Caves, Quantum-mechanical noise in an interferometer, Phys. Rev. D **23**, 1693 (1981).

[17] K. Bai, Z. Peng, H.-G. Luo, and J.-H. An, Retrieving Ideal Precision in Noisy Quantum Optical Metrology, Phys. Rev. Lett. **123**, 040402 (2019).

[18] T. Chalopin, C. Bouazza, A. Evrard, V. Makhalov, D. Dreon, J. Dalibard, L. A. Sidorenkov, and S. Nascimbene, Quantum-enhanced sensing using non-classical spin states of a highly magnetic atom, Nat. Commun. **9**, 4955 (2018).

[19] C. Invernizzi, M. Korbman, L. Campos Venuti, and M. G. A. Paris, Optimal quantum estimation in spin systems at criticality, Phys. Rev. A **78**, 042106 (2008).

[20] T.-L. Wang, L.-N. Wu, W. Yang, G.-R. Jin, N. Lambert, and F. Nori, Quantum Fisher information as a signature of the superradiant quantum phase transition, New J. Phys. **16**, 063039 (2014).

[21] I. Frérot and T. Roscilde, Quantum Critical Metrology, Phys. Rev. Lett. **121**, 020402 (2018).

[22] Y. Chu, S. Zhang, B. Yu, and J. Cai, Dynamic Framework for Criticality-Enhanced Quantum Sensing, Phys. Rev. Lett. **126**, 010502 (2021).

[23] A. W. Chin, S. F. Huelga, and M. B. Plenio, Quantum Metrology in Non-Markovian Environments, Phys. Rev. Lett. **109**, 233601 (2012).

[24] A. Zwick, G. A. Álvarez, and G. Kurizki, Criticality of environmental information obtainable by dynamically controlled quantum probes, Phys. Rev. A **94**, 042122 (2016).

[25] A. Zwick, G. A. Álvarez, and G. Kurizki, Maximizing information on the environment by dynamically controlled qubit probes, Phys. Rev. Applied **5**, 014007 (2016).

[26] Y. Matsuzaki, S. Benjamin, S. Nakayama, S. Saito, and W. J. Munro, Quantum Metrology beyond the Classical Limit

under the Effect of Dephasing, Phys. Rev. Lett. **120**, 140501 (2018).

[27] J. F. Haase, A. Smirne, J. Kołodyński, R. Demkowicz-Dobrzański, and S. F. Huelga, Fundamental limits to frequency estimation: A comprehensive microscopic perspective, New J. Phys. **20**, 053009 (2018).

[28] D. Tamascelli, C. Benedetti, H.-P. Breuer, and M. G. A. Paris, Quantum probing beyond pure dephasing, New J. Phys. **22**, 083027 (2020).

[29] W. Wu and C. Shi, Quantum parameter estimation in a dissipative environment, Phys. Rev. A **102**, 032607 (2020).

[30] W. Wu and C. Shi, Criticality-enhanced quantum sensor at finite temperature, Phys. Rev. A **104**, 022612 (2021).

[31] M. A. C. Rossi and M. G. A. Paris, Entangled quantum probes for dynamical environmental noise, Phys. Rev. A **92**, 010302(R) (2015).

[32] M. Tatsuta, Y. Matsuzaki, and A. Shimizu, Quantum metrology with generalized cat states, Phys. Rev. A **100**, 032318 (2019).

[33] K. Berrada, Non-Markovian effect on the precision of parameter estimation, Phys. Rev. A **88**, 035806 (2013).

[34] J.-G. Li, Y.-M. Wang, D. Yang, and J. Zou, Effect of prior information on noisy Bayesian frequency estimation, Phys. Rev. A **96**, 052130 (2017).

[35] W. Wu, Z. Peng, S.-Y. Bai, and J.-H. An, Threshold for a discrete-variable sensor of quantum reservoirs, Phys. Rev. Applied **15**, 054042 (2021).

[36] S. Yang, M. Al-Amri, S.-Y. Zhu, and M. S. Zubairy, Effect of counter-rotating terms on the spontaneous emission in an anisotropic photonic crystal, Phys. Rev. A **87**, 033818 (2013).

[37] H. Zheng, S. Y. Zhu, and M. S. Zubairy, Quantum Zeno and Anti-Zeno Effects: Without the Rotating-Wave Approximation, Phys. Rev. Lett. **101**, 200404 (2008).

[38] Q. Ai, Y. Li, H. Zheng, and C. P. Sun, Quantum anti-Zeno effect without rotating wave approximation, Phys. Rev. A **81**, 042116 (2010).

[39] H. Mäkelä and M. Möttönen, Effects of the rotating-wave and secular approximations on non-Markovianity, Phys. Rev. A **88**, 052111 (2013).

[40] W. Wu and M. Liu, Effects of counter-rotating-wave terms on the non-Markovianity in quantum open systems, Phys. Rev. A **96**, 032125 (2017).

[41] Y. Tanimura, Numerically "exact" approach to open quantum dynamics: The hierarchical equations of motion (HEOM), J. Chem. Phys. **153**, 020901 (2020).

[42] Y. Yan, F. Yang, Y. Liu, and J. Shao, Hierarchical approach based on stochastic decoupling to dissipative systems, Chem. Phys. Lett. **395**, 216 (2004).

[43] R.-X. Xu and Y. Yan, Dynamics of quantum dissipation systems interacting with bosonic canonical bath: Hierarchical equations of motion approach, Phys. Rev. E **75**, 031107 (2007).

[44] J. Jin, S. Welack, J. Luo, X.-Q. Li, P. Cui, R.-X. Xu, and Y. Yan, Dynamics of quantum dissipation systems interacting with fermion and boson grand canonical bath ensembles: Hierarchical equations of motion approach, J. Chem. Phys. **126**, 134113 (2007).

[45] J. Jin, X. Zheng, and Y. Yan, Exact dynamics of dissipative electronic systems and quantum transport: Hierarchical equations of motion approach, J. Chem. Phys. **128**, 234703 (2008).

[46] W. Wu, Realization of hierarchical equations of motion from stochastic perspectives, Phys. Rev. A **98**, 012110 (2018).

[47] W. Wu, Stochastic decoupling approach to the spin-boson dynamics: Perturbative and nonperturbative treatments, Phys. Rev. A **98**, 032116 (2018).

[48] S. M. Kay, *Fundamentals of Statistical Signal Processing: Estimation Theory* (Prentice-Hall, Englewood Cliffs, New Jersey, 1993).

[49] S. L. Braunstein and C. M. Caves, Statistical Distance and the Geometry of Quantum States, Phys. Rev. Lett. **72**, 3439 (1994).

[50] Y.-H. Zhang and W. Yang, Improving spin-based noise sensing by adaptive measurements, New J. Phys. **20**, 093011 (2018).

[51] J. Liu, H. Yuan, X.-M. Lu, and X. Wang, Quantum Fisher information matrix and multiparameter estimation, J. Phys. A **53**, 023001 (2020).

[52] W. Zhong, Z. Sun, J. Ma, X. Wang, and F. Nori, Fisher information under decoherence in Bloch representation, Phys. Rev. A **87**, 022337 (2013).

[53] Y.-S. Wang, C. Chen, and J.-H. An, Quantum metrology in local dissipative environments, New J. Phys. **19**, 113019 (2017).

[54] Y.-Z. Wang, S. He, L. Duan, and Q.-H. Chen, Quantum phase transitions in the spin-boson model without the counterrotating terms, Phys. Rev. B **100**, 115106 (2019).

[55] G.-Q. Zhang and J.-B. Xu, Influence of weak measurement on uncertainty relations in a quantum dissipative system, J. Opt. Soc. Am. B **36**, 205 (2019).

[56] Y.-Z. Wang, S. He, L. Duan, and Q.-H. Chen, Rich phase diagram of quantum phases in the anisotropic subohmic spin-boson model, Phys. Rev. B **101**, 155147 (2020).

[57] D. P. DiVincenzo and D. Loss, Rigorous Born approximation and beyond for the spin-boson model, Phys. Rev. B **71**, 035318 (2005).

[58] G. Burkard, Non-Markovian qubit dynamics in the presence of $1/f$ noise, Phys. Rev. B **79**, 125317 (2009).

[59] H. P. Breuer and F. Petruccione, The Theory of Open Quantum Systems (Oxford University Press, Oxford, 2002).

[60] B. Bellomo, R. Lo Franco, and G. Compagno, Non-Markovian Effects on the Dynamics of Entanglement, Phys. Rev. Lett. **99**, 160502 (2007).

[61] W. Wu and H.-Q. Lin, Quantum Zeno and anti-Zeno effects in quantum dissipative systems, Phys. Rev. A **95**, 042132 (2017).

[62] Z.-Z. Li, C.-T. Yip, H.-Y. Deng, M. Chen, T. Yu, J. Q. You, and C.-H. Lam, Approach to solving spin-boson dynamics via non-Markovian quantum trajectories, Phys. Rev. A **90**, 022122 (2014).

[63] W.-J. Yang and X.-B. Wang, Ultrastrong-coupling quantum-phase-transition phenomena in a few-qubit circuit QED system, Phys. Rev. A **95**, 043823 (2017).

[64] A. Baksic and C. Ciuti, Controlling Discrete and Continuous Symmetries in "Superradiant" Phase Transitions with Circuit QED Systems, Phys. Rev. Lett. **112**, 173601 (2014).

[65] M. Liu, S. Chesi, Z.-J. Ying, X. Chen, H.-G. Luo, and H.-Q. Lin, Universal Scaling and Critical Exponents of the Anisotropic Quantum Rabi Model, Phys. Rev. Lett. **119**, 220601 (2017).

[66] Q.-T. Xie, S. Cui, J.-P. Cao, L. Amico, and H. Fan, Anisotropic Rabi Model, Phys. Rev. X **4**, 021046 (2014).

[67] A. E. Sikkema, W. J. L. Buyers, I. Affleck, and J. Gan, Ising-Kondo lattice with transverse field: A possible f-moment Hamiltonian for URu_2Si_2, Phys. Rev. B **54**, 9322 (1996).

[68] N. Yamada, A. Sakuma, and H. Tsuchiura, Decoherence processes of a quantum two-level system coupled to a fermionic environment, J. Appl. Phys. **101**, 09C110 (2007).

[69] W.-M. Zhang, P.-Y. Lo, H.-N. Xiong, M. W.-Y. Tu, and F. Nori, General Non-Markovian Dynamics of Open Quantum Systems, Phys. Rev. Lett. **109**, 170402 (2012).

[70] A. González-Tudela and F. Galve, Anisotropic quantum emitter interactions in two-dimensional photonic-crystal baths, ACS Photonics **6**, 221 (2019).

[71] C.-J. Yang, J.-H. An, H.-G. Luo, Y. Li, and C. H. Oh, Canonical versus noncanonical equilibration dynamics of open quantum systems, Phys. Rev. E **90**, 022122 (2014).

[72] H.-B. Liu, W. L. Yang, J.-H. An, and Z.-Y. Xu, Mechanism for quantum speedup in open quantum systems, Phys. Rev. A **93**, 020105(R) (2016).

[73] A. Rançon and J. Bonart, Exact dynamics and thermalization of an open bosonic quantum system in the presence of a quantum phase transition induced by the environment, Europhys. Lett. **104**, 50010 (2013).

[74] D. P. S. McCutcheon, J. P. Paz, and A. J. Roncaglia, Comment on "General Non-Markovian Dynamics of Open Quantum Systems," Phys. Rev. Lett. **115**, 168901 (2015).

[75] D. Suess, W. T. Strunz, and A. Eisfeld, Hierarchical equations for open system dynamics in fermionic and bosonic environments, J. Stat. Phys. **159**, 1408 (2015).

[76] J. Jing and T. Yu, Non-Markovian Relaxation of a Three-Level System: Quantum Trajectory Approach, Phys. Rev. Lett. **105**, 240403 (2010).

[77] L. Diósi and L. Ferialdi, General Non-Markovian Structure of Gaussian Master and Stochastic Schrödinger Equations, Phys. Rev. Lett. **113**, 200403 (2014).

[78] D. Suess, A. Eisfeld, and W. T. Strunz, Hierarchy of Stochastic Pure States for Open Quantum System Dynamics, Phys. Rev. Lett. **113**, 150403 (2014).

[79] S. Nakajima, On Quantum Theory of Transport Phenomena: Steady Diffusion, Prog. Theor. Phys. **20**, 948 (1958).

[80] R. Zwanzig, Ensemble method in the theory of irreversibility, J. Chem. Phys. **33**, 1338 (1960).